Analytical Maximum Energy Product $(BH)_{max}$ Model for Rare-Earth-Free Magnets: Core–Shell Nanostructure

Yang-Ki Hong[1], Seok Bae[1,2], Jihoon Park[1,3], Minyeong Choi[1,4], Won-Cheol Lee[1,5], Chang-Dong Yeo[6], Md Abdul Wahed[6], Kisuk Lee[7], Haein Yim-Choi[8], and Woo-Young Lee[9]

[1]Department of Electrical and Computer Engineering and Materials Science, The University of Alabama at Tuscaloosa, Tuscaloosa, AL 35487 USA
[2]Research and Development Division, LG Innotek, Seoul 07796, Republic of Korea
[3]Korea Institute of Materials Science, Changwon, Gyeongsangnam-do 51508, Republic of Korea
[4]Research and Development Division, Hyundai Motors Company, Namyang, Gyeonggi-do 18280, Republic of Korea
[5]RF Development Team, S.LSI, Samsung Electronics, Hwaseong, Gyeonggi-do 18448, Republic of Korea
[6]Department of Mechanical Engineering, Texas Tech University, Lubbock, TX 79409 USA
[7]Department of Materials Science and Engineering, Ulsan National Institute of Science and Technology, Ulsan, Gyeongsangnam-do 44919, Republic of Korea
[8]Department of Applied Physics, Sookmyung Women's University, Seoul 04310, Republic of Korea
[9]Department of Materials Science and Engineering, Yonsei University, Seoul 03722, Republic of Korea

This article presents an analytical model for the maximum energy product [$(BH)_{max}$] in core–shell structured magnetic exchange-coupled nanomagnets. The model was validated by comparing its results to the $(BH)_{max}$ from core–shell magnets reported in the literature. This approach can serve as a universal model for designing core–shell magnets that achieve the desired $(BH)_{max}$. The $(BH)_{max}$ was determined under two distinct nucleation field (H_N) conditions: $H_N \leq M_r/2$ and $H_N \geq M_r/2$, where M_r is the remanent magnetization. In addition, two different values of magnetic hysteresis loop squareness ($SQ = M_r/M_S$) were used: 1.0 and 0.7. The soft magnetic shell's remanent magnetic flux density (B_r) ranged from 0.7 to 2.2 T, while the core diameter (D_h) varied between 50 and 250 nm in this $(BH)_{max}$ model. The low-temperature phase (LTP) MnBi-core/soft-shell nanomagnet can achieve a $(BH)_{max}$ of 40 MGOe at a B_r of 1.6 T, with a shell thickness (δ_S) of 40 nm, a D_h of 250 nm, and a volume fraction of the hard-core (f_h) of 0.43. The $(BH)_{max}$ of the hexaferrite ($SrFe_{12}O_{19}$)/soft-shell (1.9 T) nanomagnet can be improved from 5.8 (single hexaferrite phase) to 20 MGOe. This approach achieves the desired $(BH)_{max}$ of the rare-earth(RE)-free permanent magnet, thereby tackling issues related to RE mineral security and unstable supply chains.

Index Terms— **Core–shell nanomagnet, magnetic exchange coupling, maximum energy product.**

I. Introduction

PERMANENT magnets containing rare-earth (RE) minerals, which have distinctive magnetic properties, have been used in electric motors for electric vehicles (EVs) and wind power generators. However, these minerals are expensive and limited in supply, making it crucial to search for alternative materials to replace RE-based magnets in motors and generators. Alternatives to REs will benefit EVs and wind turbines, reducing greenhouse gas emissions and increasing affordability. The performance of many permanent magnets tends to degrade at high temperatures, making them unsuitable for some applications. For instance, the temperature often exceeds 423 K (150 °C) in electric motor applications, which renders such magnets ineffective. Moreover, many permanent magnets incorporate costly materials with unstable supply chains. These materials are often precious or RE metals that are limited in availability.

Received 2 April 2025; revised 3 May 2025; accepted 2 June 2025. Date of publication 5 June 2025; date of current version 27 August 2025. Corresponding authors: Y.-K. Hong and C.-D. Yeo (e-mail: ykhong@eng.ua.edu; changdong.yeo@ttu.edu).

Color versions of one or more figures in this article are available at https://doi.org/10.1109/TMAG.2025.3576933.

Digital Object Identifier 10.1109/TMAG.2025.3576933

For instance, various RE magnets, including Nd–Fe–B, Dy-doped Nd–Fe–B, Sm–Co, and Sm–Fe–N, have been utilized or considered for the motors of electric and hybrid vehicles. Nd–Fe–B generally provides the highest theoretical maximum energy product, $(BH)_{max}$, of 64 MGOe (509 KJ/m^3) and experimentally around 44 MGOe (350 KJ/m^3). The $(BH)_{max}$ is a measure of its magnetic strength.

Fig. 1 illustrates three essential magnetic properties: the magnetocrystalline anisotropy constant (K_u), saturation magnetization (M_S), and Curie temperature (T_C). Sm–Co magnets exhibit high magnetocrystalline anisotropy energy (E_K) and T_C, making them suitable for high-temperature applications. However, they are composed of expensive RE metal and cobalt. Nd–Fe–B exhibits high saturation magnetization and moderate E_K, which is suitable for electric machines, but its low T_C limits its applicability. In Fig. 1, it is evident that RE-free magnets exhibit significantly lower saturation magnetization, leading to a reduced $(BH)_{max}$. However, they possess a reasonably high K_u and T_C. The authors' group has studied the magnetic properties of RE-free ferromagnetic materials, such as τ-phase MnAl [1], [2], low-temperature phase (LTP) MnBi, and hexagonal ferrite ($SrFe_{12}O_{19}$:SrM). They discovered that the $(BH)_{max}$ values of these materials are significantly lower than those of RE ferromagnetic materials.

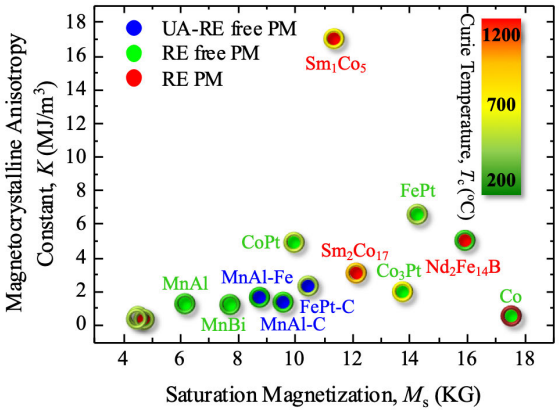

Fig. 1. Plot of magnetocrystalline anisotropy constant versus saturation magnetization with Curie temperature for permanent magnets. Note: the blue disk represents the authors' theoretical RE-free magnet, the green disk represents an RE-free magnet, and the red disk represents a commercial RE permanent magnet. The ring (shell)'s color indicates Curie temperature.

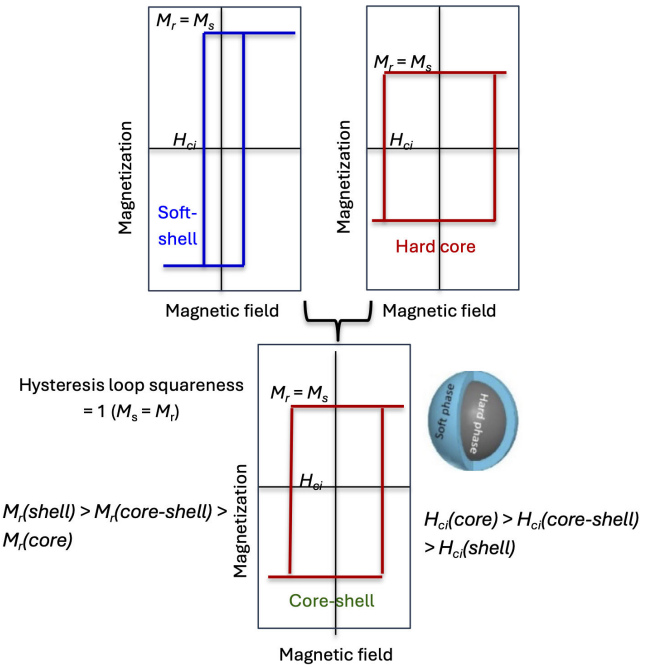

Fig. 2. Concept of the magnetic exchange coupling between hard core and soft-shell of nanomagnet and resulting magnetic hysteresis loop. M_r is the remanent magnetization, M_S is the saturation magnetization, and H_{ci} is the coercivity.

Therefore, the magnetic exchange coupling concept was introduced to address the low $(BH)_{max}$ of RE-free magnets. The possible improvement in $(BH)_{max}$ can be achieved through magnetic exchange coupling between RE-free permanent magnet core materials such as MnBi, MnAl, or hexaferrite $SrFe_{12}O_{19}$ and a soft magnetic shell. Regarding magnetothermal characteristics, the Nd–Fe–B magnet's operational temperature is limited to around 423 K (150 °C) due to its low T_C of about 583–673 K (310 °C–400 °C). Magnetization and coercivity decrease with increasing temperature and disappear at the T_C. Temperature coefficients of magnetization (α) and coercivity (β) quantify the magnetothermal stability of a permanent magnet. Thus, the RE Dy element was added to increase the operating temperature of Nd–Fe–B. This addition increased coercivity (H_{ci}). Still, it decreased M_S, leading to a lower $(BH)_{max}$ than Nd–Fe–B [3]. Therefore, the Dy substitution effect is not very significant. Furthermore, the current global supply chain of RE elements is highly vulnerable and largely controlled by a single country.

In response, a composite material comprising a hard magnetic core and a soft magnetic shell shows promise as an alternative for developing permanent magnets that do not rely on RE elements. A single-phase permanent magnet without RE elements cannot have higher M_S and H_{ci} than magnets containing RE elements like Nd–Fe–B and Sm–Co. However, it is possible to significantly improve the $(BH)_{max}$ of RE-free permanent magnets by creating magnetic exchange coupling between the hard magnetic core and soft-shell at the nanoscale, as shown in Fig. 2. The core material has a high nucleation field. In contrast, the soft-shell provides a high M_S. Magnetic exchange coupling changes the magnetic hysteresis loop by increasing M_S and decreasing H_{ci}, as shown in Fig. 2. When a hard core is magnetically coupled with a soft-shell to form a core–shell nanomagnet, the M_S of the coupled nanomagnet becomes higher than the core alone but lower than the M_S of the soft-shell. In addition, the H_{ci} of the core–shell nanomagnet is lower than that of the core but higher than that of the shell. This coupling concept enhances the $(BH)_{max}$ of permanent magnets that do not contain RE elements.

Fig. 3(a) shows the core–shell nanomagnet structure used in $(BH)_{max}$ modeling in this study. The thickness of the soft-shell (δ_S) is defined in terms of the core diameter (D_h) and the core volume fraction (f_h). Various attempts have been made to calculate or measure the $(BH)_{max}$ for core–shell nanomagnets. Westmoreland et al. [4] employed an atomistic spin model to investigate the magnetic properties of $Nd_2Fe_{14}B/\alpha$-Fe core–shell nanocomposites. They found that the exchange coupling reduces the H_{ci} and increases the M_S of the coupled system. As a result, an improvement in $(BH)_{max}$ was observed. As the volume percentage of α-Fe increases, the $(BH)_{max}$ initially increases but eventually reaches a peak and levels off. Although there is no formula for calculating $(BH)_{max}$ as a function of α-Fe volume percentage, the H_{ci} does depend on the α-Fe volume percentage. Fukunaga et al. [5] calculated the $(BH)_{max}$ for two types of RE core–shell nanomagnets. One type contains $SmCo_5$ (hard magnet) nanoparticles embedded in a soft α-Fe matrix, while the other type contains soft α-Fe particles embedded in a hard $SmCo_5$ matrix. The $(BH)_{max}$ increased with an increase in the volume fraction of α-Fe in the first type of core–shell nanomagnet, but it reached a maximum at a certain volume fraction. However, the study did not provide the formula for calculating $(BH)_{max}$. Nandwana et al. [6] conducted experiments on precious metal hard core–shell nanoparticles of biomagnetic FePt and Fe_3O_4. The results revealed that the $(BH)_{max}$ increased to 17.8 MGOe as the shell thickness increased. However, these increased levels off at 2 nm, a phenomenon known as the peaking effect. Souza et al. [7] calculated the $(BH)_{max}$ of a core–shell (Fe–Pt)-shell (Fe) nanocylinder. According to their results, the

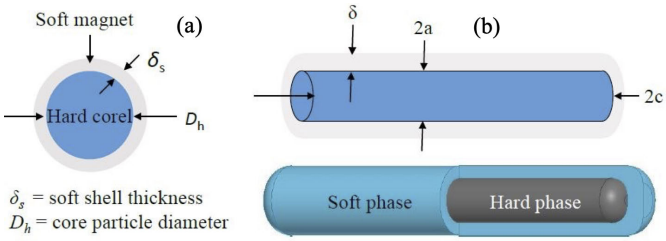

Fig. 3. Core–shell nanostructures used in $(BH)_{max}$ modeling. (a) Spherical and (b) cylindrical shape.

$(BH)_{max}$ of the FePt-@Fe core–shell nanocylinder increased as the shell thickness increased and reached its peak value of 78.39 MGOe at a shell thickness of 4 nm, after which it leveled off, exhibiting a peaking effect. Furthermore, micromagnetic simulations were conducted using the OOMMF micromagnetic simulator to estimate the $(BH)_{max}$ of the core–shell nanomagnet [8]. The simulations involved dynamically solving the Landau–Lifshitz–Gilbert equation to determine the $(BH)_{max}$ of the exchange-coupled $Sm_2Co_{17}/Fe_{65}Co_{35}$ nanocylinder. When the shell thickness of a core–shell nanocylinder is 3 nm, the $(BH)_{max}$ reaches 88 MGOe. However, beyond this point, the decrease is significant. The $(BH)_{max}$-soft-shell thickness relation also exhibits a peaking effect.

Two magnetic coupling concepts have been proposed. Skomski and Coey [9] embedded spherical soft magnetic particles in a hard magnetic matrix to explain the $(BH)_{max}$ of core–shell nanomagnet. Their modeling of $(BH)_{max}$ is based on exchange coupling. Other modeling by Kneller and Hawig [10] is based on an exchange-spring magnet, which involves embedding hard magnetic particles into a soft magnetic matrix. To achieve full magnetic exchange coupling between hard and soft magnets, the soft magnetic shell thickness should not exceed twice the domain wall thickness of the hard magnetic core. A crucial step toward the development of future permanent magnets is to model the $(BH)_{max}$ of RE-free core–shell nanomagnets. In the past, we have introduced an analytical model for the saturation magnetization (σ_S) and coercivity (H_{ci}) of spherical core–shell nanomagnets [11]. This analytical model clearly explains the relationship between the experimental σ_S or H_{ci} and the mass fraction of the hard phase in Sm_2Co_7/Fe–Co, MnAl/Fe–Co, MnBi/Fe–Co, and $BaFe_{12}O_{19}$/Fe–Co nanocomposites. However, despite advanced calculation methods, no universally accepted analytical model for $(BH)_{max}$ is currently available.

This article introduces a new, simple analytical model for the $(BH)_{max}$ of RE-free hard magnetic core/soft-shell nanomagnets. Before conducting experiments, it can be used to design magnetic exchange-coupled spherical core–shell nanomagnets with the desired high $(BH)_{max}$. The model outlines general formulas based on the geometry, dimensions, magnetic properties, and temperature of the core–shell structure.

The primary goal of this study is to develop a model that can estimate the $(BH)_{max}$ of magnetic-exchange coupled core–shell magnets. For full magnetic exchange coupling, the shell should be less than twice the Bloch domain wall thickness of the core. Equations for $(BH)_{max}$ were developed using core–shell nanomagnet particle structures, as depicted in Fig. 3(a). The core comprises magnetically hard materials such as τ-MnAl, LTP MnBi, or hexaferrite ($SrFe_{12}O_{19}$). Meanwhile, the shell is made of magnetically soft materials, including $Fe_{65}Co_{35}$, permalloy ($Fe_{20}Ni_{80}$), or Sendust (FeAlSi). However, the magnetic flux density of a soft magnet varies between 1.3 and 2.2 T (Tesla). Core–shell particles are typically spherical; however, some core–shell nanomagnets exhibit nonspherical shapes, such as needle-like or hexagonal forms. Fig. 3(b) demonstrates this point. The soft-shell thickness ranges from approximately 10 to 40 nm, which is less than twice the Bloch domain wall thickness of the core. In addition, the shell thickness is evenly distributed around the core.

II. Analytical Model

The $(BH)_{max}$ of the core–shell particle in Fig. 3(a) can be determined using the following formulas when remanent magnetization (M_r) equals M_S or 0.7 M_S. The first equation establishes the relationship between the shell thickness (δ_S) and the volume fraction of hardcore (f_h). The second equation correlates $(BH)_{max}$ with f_h for H_N less than $M_r/2$, while the third equation links $(BH)_{max}$ with f_h for H_N greater than $M_r/2$. Here, H_N represents the nucleation field. The δ_S for a spherical core–shell in Fig. 3(a) is given by the function of core diameter (D_h) and f_h: the volume of the core–shell particle is $4/3\pi R^3$, the volume of the core (hard magnet) is $4/3\pi r_h^3$. The volume of the shell (soft magnet) is $4/3\pi(R^3 - r_h^3)$, where $R = \delta + r_h$. The volume fraction of hard magnet $(f_h) = 4/3\pi r_h^3)/(4/3\pi R^3) = r_h^3/R^3$; therefore, $R^3 = r_h^3/f_h$ becomes $R = r_h/f_h^{1/3} = \delta + r_h$. As a result

$$\delta = \frac{r_h}{f_h^{1/3}} - r_h = \frac{\frac{1}{2}D_h}{f_h^{1/3}} - \frac{1}{2}D_h = \frac{1}{2}D_h\left(f_h^{-1/3} - 1\right). \quad (1)$$

There are two cases to consider when calculating the maximum value of $(BH)_{max}$. The first case is when the value of H_N is smaller than half of M_r of a core–shell particle. The second case is when the value of H_N is greater than half of M_r. Assuming that M_r equals M_S [magnetic hysteresis loop squareness (SQ = M_r/M_S = 1.0)], the following formulas can be used to calculate $(BH)_{max}$ for a core–shell particle [9], [10]:

$$M_r = f_h M_h + f_s M_s, \quad \text{when } M_s = M_r \quad (2)$$

$$\mu_0 H_N = 2\frac{f_s K_s + f_h K_h}{f_s M_s + f_h M_h} \quad (3)$$

$$(BH)_{max} = \frac{\mu_0 M_r^2}{4}, \quad \text{for } H_N > \frac{M_r}{2} \quad (4)$$

$$(BH)_{max} = \frac{\mu_0 H_N M_r}{2}, \quad \text{for } H_N < \frac{M_r}{2} \quad (5)$$

where H_N is the nucleation field, M_r is the remanence of hard plus soft phases, M_S is the saturation magnetization of soft magnetic phase, M_h is the saturation magnetization of hard magnetic phase, K_h is the magnetocrystalline anisotropy constant of hard magnetic phase, K_S is the magnetocrystalline anisotropy energy constant of soft magnetic phase, f_h is the volume fraction of hard magnetic phase, f_s is the volume fraction of soft magnetic phase, and μ_0 is $4\pi \times 10^{-7}$ N/A^2. Equations (4) and (5) can be expressed in terms of the

remanent magnetic flux density of the soft-shell ($B_{r,soft}$), the remanent magnetic flux density of the core ($B_{r,hard}$), and K_s, K_h, and f_h as follows:

$$(BH)_{max} = \frac{\left[B_{r\_soft} - f_R\left(B_{r\_soft} - B_{r\_hard}\right)\right]^2}{4} \times 10^2 \text{ MGOe}, \quad \text{for } H_N > \frac{M_r}{2}, \text{ and} \tag{6}$$

$$(BH)_{max} = \frac{4\pi\left[K_s - f_h(K_h - K_s)\right]}{10^5} \text{ MGOe}, \text{ for } H_N < \frac{M_r}{2}. \tag{7}$$

On the other hand, more realistically, assuming $M_r = 0.7M_s$ and $B_r = \mu_0 M_r$, therefore, $B_r = 0.7\mu_0 M_s$ and $B_r = 0.7B_s$, we obtained the following equation for M_r

$$M_r = \frac{f_h B_{r_{hard}} + f_s B_{r_{soft}}}{\mu_0} = \frac{f_h B_{r_{hard}} + (1 - f_h) B_{r_{soft}}}{\mu_0} \left[\frac{A}{m}\right] = \frac{0.7\left[B_{s\_soft} - f_h\left(B_{s\_soft} - B_{s\_hard}\right)\right]}{\mu_0} \left[\frac{A}{m}\right]. \tag{8}$$

Below are the calculations for the $(BH)_{max}$ for two cases as a function of saturation magnetization, the volume fraction of the hardcore, and the magnetocrystalline anisotropy constant. After some simple mathematical manipulations, we obtain (9) and (10)

For $H_N > M_r/2$,

$$\begin{aligned}(BH)_{max} &= \frac{\mu_0 M_r^2}{4} \\ &= \mu_0 \left\{0.7\left[\frac{B_{s_{soft}} - f_h\left(B_{s_{soft}} - B_{s_{hard}}\right)}{\mu_0}\right]\right\}^2 \Big/ 4 \left[T \cdot \frac{A}{m}\right] \\ &= \frac{0.49\pi\left[B_{s_{soft}} - f_h\left(B_{s_{soft}} - B_{s_{hard}}\right)\right]^2}{10^5 \times \mu_0} \\ &= \frac{4.9\pi\left[B_{s\_soft} - f_h\left(B_{s\_soft} - B_{s\_hard}\right)\right]^2}{10^6 \times \mu_0} \text{ [MGOe]}. \end{aligned} \tag{9}$$

For $H_N < (M_r/2)$

$$\begin{aligned}(BH)_{max} &= \frac{\mu_0 H_N M_r}{2} = \frac{2\left(\frac{f_s K_s + f_h K_h}{f_s M_s + f_h M_h}\right)(f_s M_s + f_h M_h)}{2} \\ &= f_s K_s + f_h K_h = (1 - f_h) K_s + f_h K_h \\ &= K_s + f_h(K_h - K_s) \\ &= \frac{4\pi\left[K_s + f_h(K_h - K_s)\right]}{10^5} \text{ [MGOe]} \end{aligned} \tag{10}$$

where B_s_soft is the B_s of the soft magnetic phase in the unit of Tesla (T), and B_h_hard is the B_s of the hard magnetic phase in the unit of Tesla [T]. The unit conversion used in those equations is

$$\left[\frac{J}{m^3}\right] = \left[\frac{kg \cdot m^2}{sec^2 m^3}\right] = \left[\frac{kg}{sec^2 m}\frac{A}{A}\right] = \left[\frac{kg}{sec^2 A}\frac{A}{m}\right] = \left[T\frac{A}{m}\right] = \left[\frac{N}{m^2}\right].$$

Next, we calculate the $(BH)_{max}$ of RE-free core–shell nanomagnets as a function of the volume fraction of hard magnetic phase (f_h) for different D_h and remanent magnetic flux density (B_r) values with various core magnets. To calculate the $(BH)_{max}$ of core–shell nanomagnets, (1), (6), (7), (9), and (10) were utilized. This study considered hard-core materials such as τ-phase MnAl, LTP MnBi, and hexagonal ferrite ($SrFe_{12}O_{19}$:SrM), while the B_r of the soft shell varied from 1.3 to 2.2 T. Experimental or theoretical data for magnetization (M) and magnetocrystalline anisotropy constant (K_u) were also incorporated. The temperature for the study was set at either 300 or 450 K, and the SQ was either 1.0 or 0.7.

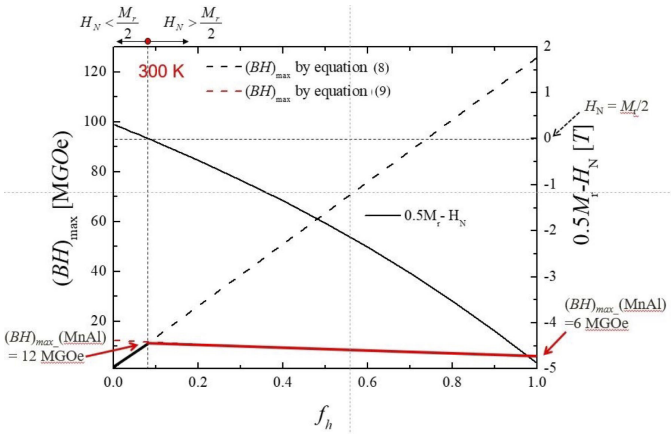

Fig. 4. $(BH)_{max}$ as a function of the volume fraction of hardcore (f_h) at 300 K for a τ-phase MnAl core–soft-shell ($Fe_{20}Ni_{80}$: permalloy) nanomagnet and ($1/2M_r - H_N$) as a function of f_h.

III. Model Applications

Fig. 4 depicts the $(BH)_{max}$ of a τ-phase MnAl/permalloy ($Fe_{20}Ni_{80}$) core–shell nanomagnet as a function of the volume fraction of the hard core (f_h). The τ-phase MnAl core has a magnetic flux density ($B_{s,hard}$) of 0.7 T and a K_h of 1 MJ/m^3 [12], while the soft magnetic permalloy shell has a magnetic flux density ($B_{s,soft}$) of 1 T and a K_S of 0.01 MJ/m^3. Fig. 4 also shows the relationship between ($M_r/2 - H_N$) and f_h. Equations (6) and (7) were used to estimate the $(BH)_{max}$ of a τ-phase MnAl-permalloy core–shell nanomagnet for H_N greater than $M_r/2$ and H_N less than $M_r/2$, respectively. It is worth noting that the $(BH)_{max}$ is around 12 MGOe when the H_N equals $M_r/2$ and f_h is 8%. In contrast, the $(BH)_{max}$ of a single-phase τ-MnAl magnet, with a f_h of 100%, is approximately 6 MGOe, as illustrated in Fig. 4. The $(BH)_{max}$ of a single-phase τ-MnAl magnet can be determined at $f_h = 1$, which means 100% of the magnet is made up of the core. On the other hand, when the f_h is 0.0, the magnet is 100% made up of the soft magnet. In this case, H_N, therefore coercivity, is almost negligible, which results in nearly zero $(BH)_{max}$, as seen in Fig. 4. Therefore, the core–shell nanomagnet becomes a soft magnet.

In this research, we aimed to predict the $(BH)_{max}$ of core–shell nanomagnets. We used RE-free core magnetic materials with two different squareness values (SQ = M_r/M_S = 1.0 or 0.7) of the magnetic hysteresis loop and various B_r (1.3–2.2 T) of a soft-shell at two different temperatures (300 and 450 K).

We specifically examined three RE-free core ferromagnetic materials: τ-phase MnAl, LTP MnBi, and hexaferrite ($BaFe_{12}O_{19}$:SrM). The first two ferromagnetic materials are laboratory products, whereas SrM is a commercial product. We calculated the $(BH)_{max}$ at 300 and 450 K using two different values for the squareness of the magnetic hysteresis loop (SQ $= M_r/M_S$), 1.0 and 0.7. It is generally preferable for the soft-shell thickness (δ_S) to be thinner than about twice the Bloch domain wall thickness (δ_d) of the core to ensure efficient exchange magnetic coupling between the core and shell [10]. The δ_s of a τ-phase MnAl core–soft-shell nanomagnet with a B_r of 1.3–2.2 T should be less than 30 nm for optimal performance. This is because the δ_d of the τ-phase MnAl core is approximately 15 nm [13]. M_h, K_h, and K_s are obtained from [12], [14], and [15].

The $(BH)_{max}$ of the τ-phase MnAl core–soft-shell nanomagnet was obtained at 300 and 450 K with two different SQ of 1.0 and 0.7 using (1), (6), (7), (9), and (10). Fig. 5(a) depicts the $(BH)_{max}$ of the τ-phase MnAl core–soft-shell nanomagnet as a function of f_h. Despite the shell's B_r, the $(BH)_{max}$ reaches a peak value, showing a peak phenomenon. When a nanomagnet made of τ-phase MnAl/CoFe (2.2 T) is fully exchange-coupled at a D_h of 250 nm and a δ_S of 28 nm, with an f_h of about 52% and an SQ value of 1.0, its $(BH)_{max}$ reaches approximately 50 MGOe at 300 K. The $(BH)_{max}$ of the core–shell magnet is around 400% higher than the 12.3 MGOe of the single-phase τ-phase MnAl magnet when the f_h is 1.0.

Next, the squareness (SQ $= M_r/M_S$) of the magnetic hysteresis loop for a τ-phase MnAl core with a soft-shell ($B_r = 1.3$–2.2 T) nanomagnet was adjusted from 1.0 to 0.7 to make the hysteresis loop more realistic. Equations (9) and (10) were utilized to obtain the $(BH)_{max}$ in Fig. 5(b).

The $(BH)_{max}$ of the τ-phase MnAl-CoFe (2.2 T) core–shell nanomagnet reaches about 35 MGOe, with a SQ of 0.7, when exchange coupling is present at a D_h of 70 nm, with a δ_S of around 20 nm and a f_h of approximately 30%. In single-phase MnAl (with $f_h = 100\%$), the $(BH)_{max}$ drops from 12.3 to 6 MGOe at 300 K as the SQ decreases from 1.0 to 0.7, as shown in Figs. 5(a) and 6(b). When the SQ changes from 1.0 to 0.7, the $(BH)_{max}$ shifts to a lower value for all volume fractions of the hardcore, as shown in Fig. 5(a) and (b). This suggests that SQ plays a crucial role in manufacturing permanent magnets. The $(BH)_{max}$ follows a peaking phenomenon, increasing and decreasing as the f_h increases for all B_r. The peak shifts toward the higher f_h as B_r increases. This aligns with the $(BH)_{max}$ behavior shown in Fig. 5(a). It is important to note that all $(BH)_{max}$ values are lower than those with an SQ of 1.0.

Like an internal combustion engine (ICE), an EV motor must be properly cooled to operate efficiently and safely at temperatures below 368 K. Failure to do so can result in overheating. To address this issue, the $(BH)_{max}$ of the τ-phase MnAl core–soft-shell nanomagnet (SQ $= 1.0$) was calculated at 450 K, a temperature sufficiently high to prevent it from reaching the critical 423 K (150 °C).

In Fig. 5(c), the $(BH)_{max}$ of the τ-phase MnAl-CoFe core–shell nanomagnet reaches approximately 40 MGOe at 450 K when there is full exchange coupling at a D_h of 250 nm, a δ_S of around 20 nm, an f_h of 60%, and an SQ of 1.0. Regardless of B_r, the $(BH)_{max}$ increases as the f_h increases, reaching a peak value and exhibiting a peak phenomenon. As observed in Figs. 5(a) and 6(b), the peak of $(BH)_{max}$ shifts to a higher f_h as the B_r increases. It is noted that the $(BH)_{max}$ of the τ-phase MnAl single phase ($f_h = 1.0$) decreases to 9.9 MGOe from 12.3 MGOe at 300 K in Fig. 5(b).

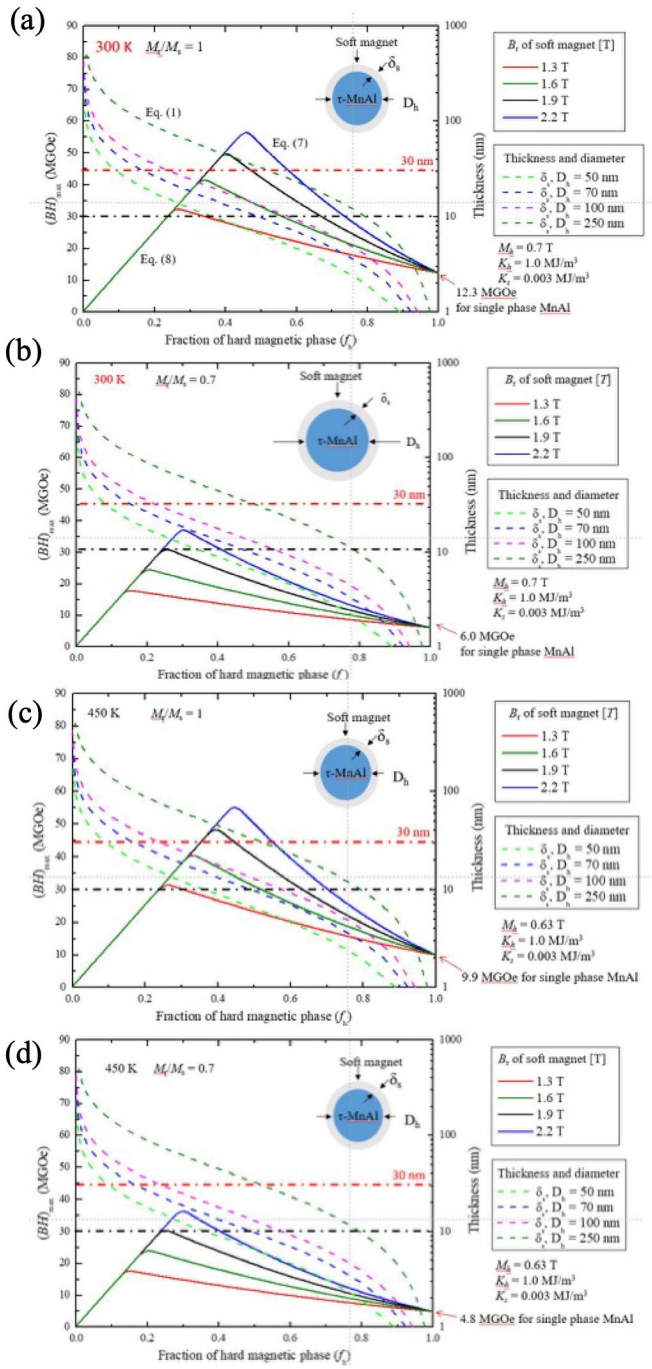

Fig. 5. $(BH)_{max}$ as a function of the volume fraction of hard core (f_h) for a τ-phase MnAl core–soft-shell nanomagnet at (a) 300 K and the SQ (M_r/M_S) is 1.0, (b) 300 K and the SQ (M_r/M_S) is 0.7, (c) 450 K and the SQ (M_r/M_S) is 1.0, and (d) 450 K and the SQ (M_r/M_S) is 0.7. For all the cases the remanent magnetic flux density (B_r) is in the range of 1.3–2.2 T. The shell thickness (δ_S) must be less than 30 nm ($2 \times \delta_d$) for fully magnetic exchange coupling. The M_h at 450 K is 0.63 T, smaller than 0.70 T at 300 K.

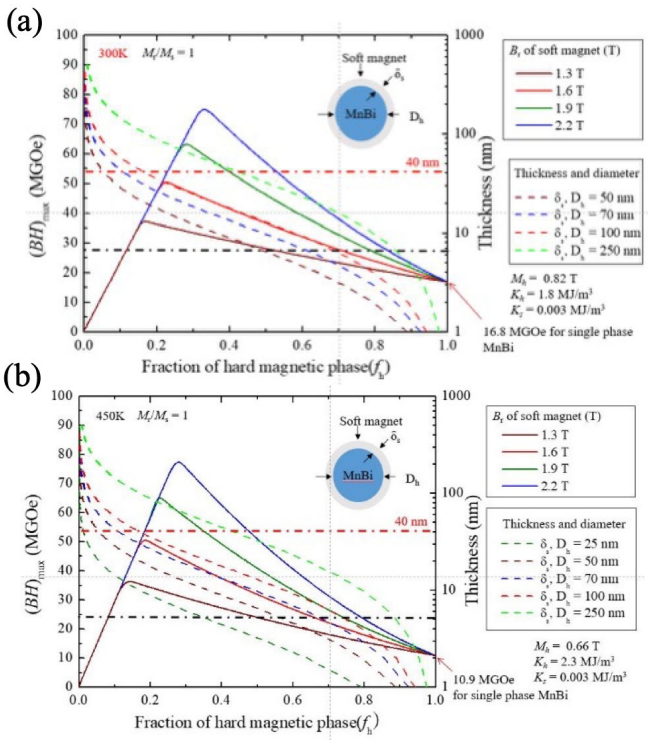

Fig. 6. $(BH)_{max}$ as a function of f_h for a LTP MnBi core–soft-shell nanomagnet at (a) 300 and (b) 450 K. For both cases, the SQ (M_r/M_S) is 1.0, and the remanent magnetic flux density (B_r) of soft-shell is in the range of 1.3–2.2 T. The M_h at 450 K is 0.66 T, smaller than 0.82 T at 300 K.

In Fig. 5(d), we change the SQ to 0.7 from 1.0 for calculating $(BH)_{max}$ at 450 K. The $(BH)_{max}$ of the core–shell nanomagnet significantly decreased compared to the $(BH)_{max}$ (SQ = 1.0) shown in Fig. 5(c). The $(BH)_{max}$ of a τ-phase MnAl core (SQ = 0.7) is only 4.8 MGOe, which is significantly lower than 9.9 MGOe (SQ = 1.0) at 450 K in Fig. 5(c). Also, achieving a $(BH)_{max}$ of 40 MGOe (SQ = 1.0) is not possible when the SQ is 0.7. However, 30 MGOe can be attained when D_h is 100 nm, δ_S is about 20 nm, and f_h is approximately 40%. Even at 450 K, the $(BH)_{max}$ (SQ = 1.0) remains higher than 4.8 MGOe (SQ = 0.7). The $(BH)_{max}$ peak is lower than 300 K because the B_r (0.63 T) is smaller than 0.7 T at 300 K. It is worth noting that the SQ has a more significant impact on $(BH)_{max}$ than temperature, as demonstrated in Fig. 5.

Permanent magnets are commonly used in high-temperature applications. Nd–Fe–B magnets are unsuitable for such environments because they become magnetically unstable due to their low T_C and a significant negative temperature coefficient of coercivity (β). On the other hand, LTP MnBi has a positive β, indicating that its coercivity increases with rising temperature. This makes it ideal for high-temperature applications. Thus, we have examined RE-free LTP MnBi and hexaferrite, which possess a positive β. However, RE-free LTP MnBi and hexaferrite have a lower saturation magnetization than RE permanent magnets. It is possible to overcome the low-magnetization disadvantage of LTP MnBi and hexaferrite by coupling them with a high-saturation magnetization soft shell through magnetic exchange. Fig. 6(a) shows the $(BH)_{max}$ at 300 K of LTP MnBi core–soft-shell nanomagnet as a function of f_h. When exchange coupling exists at a D_h of 250 nm, a δ_S of about 30 nm, and a f_h of about 55%, the $(BH)_{max}$ of LTP MnBi core–shell (2.2 T) nanomagnet is approximately 50 MGOe at 300 K. The values of M_h, K_h, and K_S were obtained from [10], [11], and [12].

To examine the thermal behavior of $(BH)_{max}$ shown in Fig. 6(a), the temperature was raised from 300 to 450 K. Fig. 6(b) shows the $(BH)_{max}$ at 450 K for an LTP MnBi core–soft-shell nanomagnet with SQ = 1.0. It is worth noting that LTP MnBi exhibits a positive β, meaning it has a higher magnetocrystalline anisotropy constant than 300 K. The shape of the $(BH)_{max}$ curve remained unchanged compared to the shape in Fig. 6(a). The $(BH)_{max}$ is 50 MGO when full exchange coupling occurs at D_h = 250 nm, δ_S is approximately 30 nm, f_h is about 50%, and B_r is 2.2 T. For single phase (f_h = 100%) LTP MnBi, the $(BH)_{max}$ is 10.9 MGOe at 450 K, much lower than 16.8 MGOe at 300 K in Fig. 6(a).

Regarding the hexaferrite ($SrFe_{12}O_{19}$:SrM) core, a study conducted by Park et al. [16] found that it is challenging to improve the $(BH)_{max}$ of the cost-effective and chemically stable hexaferrite beyond 5.8 MGOe. This is due to the complex magnetic spin structure resulting from five distinct magnetic sites within the SrM unit cell. The hexaferrite, like LTP MnBi, exhibits a positive β, making it suitable for high-temperature applications. Despite its low saturation magnetization, this can be improved through magnetic exchange coupling between the hard SrM core and the soft magnetic shell, enhancing its $(BH)_{max}$.

In Fig. 7(a), the magnetic exchange coupling between SrM and the soft-shell (1.9 T) results in an increase in the $(BH)_{max}$ from 5.8 MGOe of single-phase SrM (f_h = 100%) to 20 MGOe at 300 K. The following magnetic properties for the core and shell were used in calculating $(BH)_{max}$:M_h = 0.48 T [17], K_h = 0.33 MJ/m^3 [18], K_S = 0.003 MJ/m^3 [15], δ_d = 14 nm [19], and SQ = 1. The thickness of the shell cannot exceed $2\delta_d$, which is 28 nm for full magnetic exchange coupling. The $(BH)_{max}$ shape is in line with core–shell nanomagnets, such as MnAl and MnBi, exhibiting a peaking phenomenon.

The following magnetic properties were used to test the thermal behavior of the $(BH)_{max}$ at 450 K: M_h = 0.32 T, K_h = 0.20 MJ/m^3, K_S = 0.003 MJ/m^3, and SQ = 1.0. Fig. 7(b) shows that the $(BH)_{max}$ value for a single-phase SrM decreased to 2.6 MGOe from 5.8 MGOe at 300 K. The shape of $(BH)_{max}$ versus f_h curve is identical to that at 300 K. According to Fig. 7(b), an SrM core–shell magnet can be designed with a 250 nm diameter, a shell thickness of around 20 nm, a core volume fraction of approximately 65%, and a remanence of 1.6 T for 15 MGOe of $(BH)_{max}$ at 450 K.

It was found that the $(BH)_{max}$ shape of the core–shell magnet is independent of magnetic properties and core–shell dimensions. Magnetic exchange coupling between the hard-core and soft-shell can overcome the disadvantages of RE-free permanent magnets. The proposed $(BH)_{max}$ model can guide the design of an RE-free hard-core–shell magnet with the desired $(BH)_{max}$ and produce RE-free permanent magnets. Fabricating a nanomagnet with a uniform soft-shell around a hard core can be challenging. However, various techniques

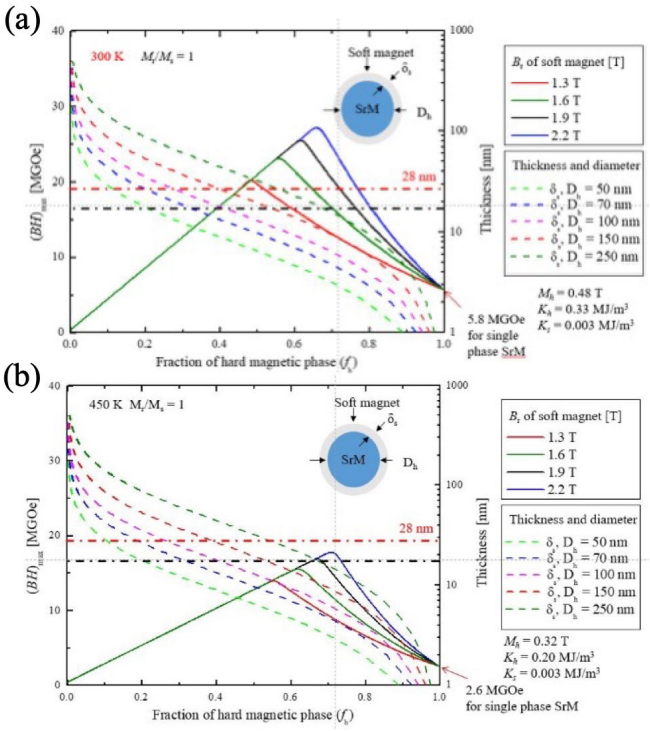

Fig. 7. $(BH)_{max}$ as a function of f_h for a hexaferrite (SrM) core- and soft-shell nanomagnet at (a) 300 and (b) 450 K. For both cases, the SQ (M_r/M_S) is 1.0, and the remanent magnetic flux density (B_r) of soft-shell is in the range of 1.3–2.2 T. The M_h at 450 K is 0.32 T, smaller than 0.48 at 300 K.

are available, such as electroless plating, chemical and physical synthesis, and embedding core–shell nanomagnets in a polymeric matrix, which can successfully produce core–shell nanomagnetic materials.

Any model can be validated by comparing its outputs to experimental or other computational datasets that align with the simulated scenario. In Sections IV and V, we validated our proposed $(BH)_{max}$ model by comparing it with experimental and computational results of core–shell nanomagnets from the literature.

IV. Validation of the $(BH)_{max}$ Model for Single-Phase Magnets

The results in this study confirm that designing a core–shell structure with a specific core diameter, shell thickness, and magnetic flux density under full exchange coupling can achieve a higher $(BH)_{max}$ than a single-phase core magnet. The proposed $(BH)_{max}$ model is validated by comparing the results in this study with those reported in other studies.

First, we tested our $(BH)_{max}$ model using reported $(BH)_{max}$ values for single-phase and hard magnetic core–soft composites. The experimental or theoretical $(BH)_{max}$ of single-phase τ-MnAl, LTP MnBi, and hexaferrite core magnets were compared with our $(BH)_{max}$ model for $f_h = 1.0$ (100% core magnet), which was calculated using (6) or (9).

The $(BH)_{max}$ of a single-phase τ-phase MnAl was calculated to be 12.64 MGOe [2], However, according to Coey, the theoretical upper limit of $(BH)_{max}$ for the τ-phase MnAl is 14 MGOe [20]. The τ-MnAl has $(BH)_{max}$ value of 19.2 MGOe (153 kJ/m^3) for a calculated M_S value of 137 emu/g [21]. The $(BH)_{max}$ of 12.3 MGOe at $f_h = 1.0$ (single MnAl phase) in Fig. 5(a) is in good agreement with the reported theoretical and experimental values [13], [15], [22]. We confirm the accuracy of the proposed $(BH)_{max}$ model for single-phase τ-MnAl.

As shown in Fig. 5(a) and (b), the SQ of MnAl/soft-shell nanomagnets directly affects the $(BH)_{max}$. When the SQ drops from 1.0 to 0.7, $(BH)_{max}$ decreases from 12.3 to 6.0 MGOe. The presence of secondary phases, such as β-Mn and γ_2-Al_8Mn_5, in the τ-phase of MnAl causes the SQ to decrease. Therefore, improving the stability of the τ-phase is crucial for increasing $(BH)_{max}$ and reaching the theoretical value. This can be achieved by developing an advanced synthetic process that reduces or eliminates the secondary phases from the Mn–Al alloy, therefore meeting the theoretical $(BH)_{max}$ value.

LTP MnBi has garnered significant attention for its high-temperature applications in permanent magnets, owing to its high magnetocrystalline energy, Curie temperature, and positive β coefficient. The $(BH)_{max}$ of LTP MnBi is theoretically 17 MGOe [23]. However, due to unstable LTP and deformation of MnBi crystallites, the experimental $(BH)_{max}$ is lower than this value. To calculate $(BH)_{max}$ of LTP MnBi at 300 K, Park et al. [24] used first-principles calculations and the Brillouin function and found it to be 17.7 MGOe. High-purity MnBi film, which has a perfect c-axis orientation and is 100 nm thick, shows a $(BH)_{max}$ of 16.3 MGOe at 300 K [25]. Tang et al. [26] reported 8.9 MGOe of bulk MnBi at 300 K. This low $(BH)_{max}$ is due to an incomplete LTP of MnBi. Excitingly, Sharma et al. [22] observed experimental 14.8 MGOe of $(BH)_{max}$ at 300 K for LTP Mn–Bi. All these reported experimental and theoretical $(BH)_{max}$ of single-phase LTP Mn–Bi agree to 16.8 MGOe at $f_h = 1.0$ of our $(BH)_{max}$ model, as shown in Fig. 6(a). Therefore, our $(BH)_{max}$ model is validated, confirming its accuracy.

Due to their cost-effectiveness and chemical stability, hexaferrite (SrM) permanent magnets are increasingly used in low-power electric machines. Even wind generators now employ these magnets. A single-phase ferrite permanent magnet's theoretical $(BH)_{max}$ at 300 K was estimated to be 5.9 MGOe by first-principles calculation and Brillouin function [16]. The commercial hexaferrite permanent magnet has a $(BH)_{max}$ of 5.5 MGOe [17]. In a recent experiment, Huang et al. [27] obtained a $(BH)_{max}$ of 5.23 MGOe for a single-phase hexaferrite at 300 K. The reported experimental and theoretical $(BH)_{max}$ values of single-phase SrM agree with the 5.8 MGOe value at $f_h = 1.0$, as shown in Fig. 7(a).

All reported values for $(BH)_{max}$ in the literature for single-phase τ-MnAl, LTP MnBi, and hexaferrite (SrM) agree with the $(BH)_{max}$ values at 100% f_h in our proposed model for $(BH)_{max}$ of core–shell nanomagnets.

V. Validation of the $(BH)_{max}$ Model for Core–Shell Nanomagnets (Two Phase)

To validate our proposed analytical $(BH)_{max}$ model, we compared the $(BH)_{max}$ values of the core–shell nanomagnets reported in the literature with those predicted by our proposed $(BH)_{max}$ model in this work.

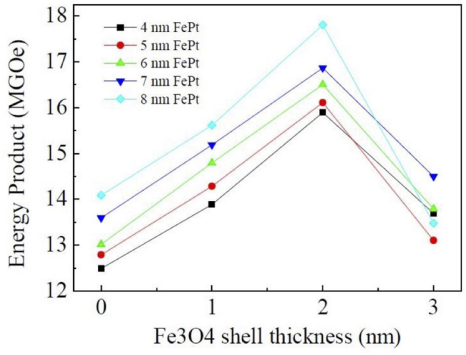

Fig. 8. $(BH)_{max}$ for a FePt/Fe_3O_4 core–shell as a function of Fe_3O_4 thickness [6].

Fukunaga et al. [5] have conducted a micromagnetic simulation on a $SmCo_5/\alpha$-Fe nanocomposite magnet to estimate $(BH)_{max}$. The results confirm that $(BH)_{max}$ increases as the fraction of soft α-Fe shell increases, regardless of core–shell volume or magnetic properties. The maximum value of $(BH)_{max}$ can be reached at a specific fraction, known as the peaking phenomenon. This trend is in line with the analytical $(BH)_{max}$ model shown in Fig. 4. Hence, the results of the micromagnetic simulation also confirm the validity of our $(BH)_{max}$ model.

In a study by Nandwana et al. [6], a biomagnetic FePt/Fe_3O_4 core–shell was synthesized and characterized for its $(BH)_{max}$. Fig. 8 illustrates the influence of Fe_3O_4 thickness on $(BH)_{max}$. The findings confirm that $(BH)_{max}$ rises as the thickness of Fe_3O_4 increases and reaches a maximum. The research found that the highest value of $(BH)_{max}$ was 17.8 MGOe at a thickness of 2 nm. This is 36% more than the $(BH)_{max}$ value of the single-phase FePt. However, beyond 2 nm, the $(BH)_{max}$ value drops rapidly, indicating a peak effect. This trend is consistent with our proposed $(BH)_{max}$ model.

Cui et al. [28] studied magnetic exchange-coupled nanofilms to investigate their $(BH)_{max}$. The $(BH)_{max}$ of MnBi/Co_xFe_{1-x} bilayer ($x = 1$) was found to be 25 MGOe (200 kJ/m^3) at 300 K, as shown in Fig. 9(a). The $(BH)_{max}$ of MnBi/Co_xFe_{1-x} bilayer increases with the thickness of the soft layer and reaches a peak value of $(BH)_{max}$ at a thickness of 3 nm, independent of the x value. Beyond this point, the $(BH)_{max}$ decreased rapidly. Notably, the $(BH)_{max}$ of a single-phase MnBi hard film was 12.3 MGOe (100 kJ/m^3). This value is close to 16.8 MGOe for $f_h = 1$ (100% hard phase) in Fig. 6(a). This $(BH)_{max}$ behavior is effectively explained by our $(BH)_{max}$ model as depicted in Figs. 4–7.

Kim et al. [29] used the finite differential micromagnetic solver MuMax3 to calculate the $(BH)_{max}$ of a Sm_2Co_{17}/Fe–Co cylindrical core/shell structure. The findings are presented in Fig. 9(b). The $(BH)_{max}$ increases as the fraction of soft-shell (f_s) decreases and reaches a peak value, regardless of the diameter-to-length (D/L) ratio. These results support our analytical model for $(BH)_{max}$.

When L_{10}-FePt/Co core–shell nanoparticles are embedded in epoxy resin and oriented under an external field, the $(BH)_{max}$ increases as the shell thickness increases, as shown in Fig. 10(a) [30]. The study found that the highest $(BH)_{max}$ value of 7.1 MGOe was obtained when the shell thickness was 1 nm, representing an 80% improvement compared to the single-phase $L1_0$-FePt core. This result confirms our analytical model of $(BH)_{max}$ presented in Figs. 5–7. The plots also exhibit a similar peaking phenomenon in the $(BH)_{max}$ versus volume fraction of the hard core.

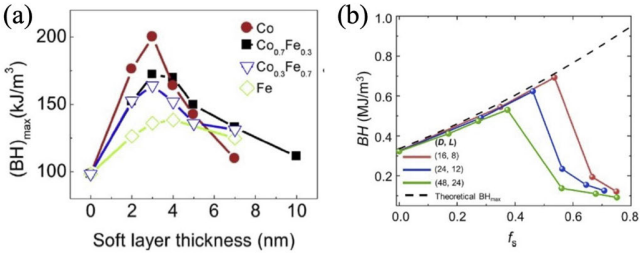

Fig. 9. (a) $(BH)_{max}$ of MnBi/Co_xFe_{1-x} bilayers for different soft-layer compositions and thicknesses [28]. (b) $(BH)_{max}$ of Sm_2Co_{17}/Fe–Co core–shell cylinder as a function of the soft-phase volume fraction f_s at different scales [29].

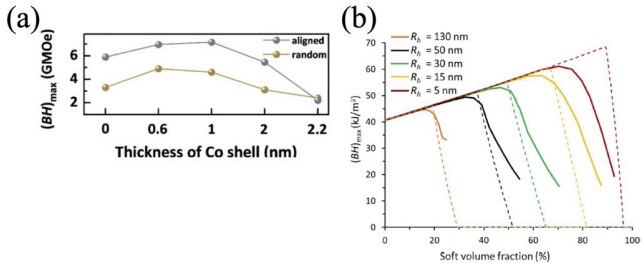

Fig. 10. (a) $(BH)_{max}$ as a function of Co shell thickness [30]. (b) Dependence of $(BH)_{max}$ on soft volume fraction at fixed hard core radii. The variation of the soft volume fraction results from incremental change of the thickness of the soft-shell [31].

Finally, we discuss the $(BH)_{max}$ of hard (hexaferrite)-soft shell magnets. Despite their low saturation magnetization and, therefore, low $(BH)_{max}$, these magnets have been used in low-power electric machines. However, they are still preferred due to their chemical stability and low cost per kilogram. Core–shell magnets were developed using the concept of magnetic exchange coupling to enhance saturation magnetization. Trasitaru et al. [31] used the micromagnetic finite element model to calculate $(BH)_{max}$ for hard hexaferrite core/soft spinel ferrite shell. The $(BH)_{max}$ is shown in [31, Fig. 3] as a function of the soft volume fraction for different core radii. It has been observed that the maximum value of $(BH)_{max}$ exists regardless of the core radius. However, as the core radius decreases, this maximum value shifts toward a higher $(BH)_{max}$ value. It is worth noting that this pattern resembles the (BH) of our model. When the magnetic core–shell nanomagnet comprises 100% hexaferrite, the $(BH)_{max}$ at $f_s = 0.0$ equals 43 kJ/m^3 (approximately 5.3 MGOe). This value is in good agreement with the $(BH)_{max}$ value of 5.8 MGOe at $f_h = 1.0$ (which represents a 100% hexaferrite core magnet), as shown in Fig. 7(a). In addition, this value of $(BH)_{max}$ is consistent with the value of 5.9 MGOe reported by Park et al. [16].

VI. Conclusion

Our proposed model seeks to enhance the maximum energy product $(BH)_{max}$ of RE-free magnets by leveraging magnetic

exchange coupling between a hard core and a soft-shell. This model effectively accounts for all observed $(BH)_{max}$ behaviors of the core–shell magnet, eliminating the need for excessive computation time and energy. It can serve as a universal framework for designing permanent magnets with the desired $(BH)_{max}$.

The thickness of the shell is less than 40 nm or less than twice the Bloch domain wall thickness of the core. The $(BH)_{max}$ of a core–shell nanomagnet made of τ-phase MnAl-CoFe (2.2 T) can reach up to 35 MGOe if there is full magnetic exchange coupling. A MnBi nanomagnet with a soft shell (1.6 T) can achieve a high $(BH)_{max}$ of 40 MGOe. Furthermore, magnetic exchange coupling increased the $(BH)_{max}$ of a hexaferrite ($SrFe_{12}O_{19}$)-soft-shell (1.9 T) nanomagnet from 5.8 to 20 MGOe.

ACKNOWLEDGMENT

Yang-Ki Hong received support from the US National Science Foundation (NSF) IUCRC under Grant No. 2137275 and the E. A. "Larry" Drummond Endowment at the University of Alabama, Tuscaloosa, Alabama 35487, USA.

DECLARATION OF COMPETING INTEREST

The authors declare no competing financial interest.

REFERENCES

[1] S. Kim et al., "Composition and property optimization of rare-earth-free Mn-Al-C magnet by phase stability and magnetic behavior analysis," *J. Alloys Compounds*, vol. 919, Oct. 2022, Art. no. 165773, doi: 10.1016/j.jallcom.2022.165773.

[2] J. H. Park et al., "Saturation magnetization and crystalline anisotropy calculations for MnAl permanent magnet," *J. Appl. Phys.*, vol. 107, no. 9, pp. 10–13, May 2010, doi: 10.1063/1.3337640.

[3] K. Takagi, Y. Hirayama, S. Okada, W. Yamaguchi, and K. Ozaki, "Novel powder processing technologies for production of rare-Earth permanent magnets," *Sci. Technol. Adv. Mater.*, vol. 22, no. 1, pp. 150–159, Dec. 2021, doi: 10.1080/14686996.2021.1875791.

[4] S. C. Westmoreland et al., "Atomistic simulations of α-Fe/$Nd_2Fe_{14}B$ magnetic core/shell nanocomposites with enhanced energy product for high temperature permanent magnet applications," *J. Appl. Phys.*, vol. 127, no. 13, Apr. 2020, Art. no. 133901, doi: 10.1063/1.5126327.

[5] H. Fukunaga, R. Horikawa, M. Nakano, T. Yanai, T. Fukuzaki, and K. Abe, "Computer simulations of the magnetic properties of Sm-Co/α-Fe nanocomposite magnets with a core-shell structure," *IEEE Trans. Magn.*, vol. 49, no. 7, pp. 3240–3243, Jul. 2013, doi: 10.1109/TMAG.2013.2247030.

[6] V. Nandwana, G. S. Chaubey, K. Yano, C.-B. Rong, and J. P. Liu, "Bimagnetic nanoparticles with enhanced exchange coupling and energy products," *J. Appl. Phys.*, vol. 105, no. 1, Jan. 2009, Art. no. 014303, doi: 10.1063/1.3054441.

[7] R. M. Souza, Y. S. M. Santos, L. L. Oliveira, M. S. Nunes, A. L. Dantas, and A. S. Carriço, "Energy product of cylindrical FePt@$CoFe_2$ and FePt@Fe nanoparticles," *AIP Adv.*, vol. 9, no. 12, Dec. 2019, Art. no. 125131, doi: 10.1063/1.5129535.

[8] Z. Yang et al., "Effects of shape anisotropy on hard–soft exchange-coupled permanent magnets," *Nanomaterials*, vol. 12, no. 8, p. 1261, Apr. 2022, doi: 10.3390/nano12081261.

[9] R. Skomski and J. M. D. Coey, "Giant energy product in nanostructured two-phase magnets," *Phys. Rev. B, Condens. Matter*, vol. 48, no. 21, pp. 15812–15816, Dec. 1993.

[10] E. F. Kneller and R. Hawig, "The exchange-spring magnet: A new material principle for permanent magnets," *IEEE Trans. Magn.*, vol. 27, no. 4, pp. 3560–3588, Jul. 1991, doi: 10.1109/20.102931.

[11] J. Park et al., "A simple analytical model for magnetization and coercivity of hard/soft nanocomposite magnets," *Sci. Rep.*, vol. 7, no. 1, pp. 1–5, Jul. 2017, doi: 10.1038/s41598-017-04632-6.

[12] K. Kamino, T. Kawaguchi, and M. Nagakura, "Magnetic properties of MnAl system alloys," *IEEE Trans. Magn.*, vol. MAG-2, no. 3, pp. 506–510, Sep. 1966, doi: 10.1109/TMAG.1966.1065887.

[13] G. F. Korznikova, "Domain structures of ultrafine grained ferromagnets achieved by severe plastic deformation or melt quenching," *J. Microsc.*, vol. 239, no. 3, pp. 239–244, Sep. 2010, doi: 10.1111/j.1365-2818.2010.03372.x.

[14] N. I. Vlasova, G. S. Kandaurova, and Y. A. S. Shur, "Magnetic properties and crystal structure of Mn-Ai alloys," *Phys. Met. Metallogr.*, vol. 51, p. 207, May 1981.

[15] Y. Zhang and D. G. Ivey, "Characterization of Co-Fe and Co-Fe-Ni soft magnetic films electrodeposited from citrate-stabilized sulfate baths," *Mater. Sci. Eng., B*, vol. 140, nos. 1–2, pp. 15–22, May 2007, doi: 10.1016/j.mseb.2007.03.004.

[16] J. Park et al., "Maximum energy product at elevated temperatures for hexagonal strontium ferrite ($SrFe_{12}O_{19}$) magnet," *J. Magn. Magn. Mater.*, vol. 355, pp. 1–6, Apr. 2014, doi: 10.1016/j.jmmm.2013.11.032.

[17] TDK Corp. (2014). *TDK Corporation, TDK Catalog 2014*. [Online]. Available: https://product.tdk.com/info/en/catalog/datasheets/magnet_fb_summary_en.pdf

[18] O. M. H. Landolt, R. Boörnstein, K. H. Hellwege, D. Bimberg, M. Schulz, and H. Weiss, "Landolt–Börnstein numerical data and functional relationships in science and technology group 3," in *Crystal Solid State Physics*, vol. 17. Berlin, Germany: Springer, 1982. [Online]. Available: https://search.worldcat.org/title/Landolt-Bornstein-numerical-data-and-functional-relationships-in-science-and-technology.-Group-3-Crystal-and-solid-state-physics.-Vol.-17-Semiconductors/oclc/605929230

[19] M. Ziese and M. J. Thornton, *Spin Electronics*. Berlin, Germany: Springer, 2001, doi: 10.1007/3-540-45258-3.

[20] J. M. D. Coey, "Hard magnetic materials: A perspective," *IEEE Trans. Magn.*, vol. 47, no. 12, pp. 4671–4681, Dec. 2011, doi: 10.1109/TMAG.2011.2166975.

[21] A. Edström, J. Chico, A. Jakobsson, A. Bergman, and J. Rusz, "Electronic structure and magnetic properties of $L1_0$ binary alloys," *Phys. Rev. B, Condens. Matter*, vol. 90, no. 1, pp. 1–5, Jul. 2014, doi: 10.1103/physrevb.90.014402.

[22] S. K. Sharma, D. Pradhan, and S. Ram, "A core-shell magnet $Mn_{70}Bi_{30}$ grown at seeds in magnetic fields and its impacts on its spin-dynamics, Curie point and other tailored properties," *Nanotechnology*, vol. 34, no. 33, Aug. 2023, Art. no. 335703, doi: 10.1088/1361-6528/acd34c.

[23] R. G. Pirich and D. J. Larson Jr., "Directional solidification and densification of permanent magnets having single domain size MnBi particles," U.S. Patent 4 784 703, Nov. 15, 1988.

[24] J. Park, Y.-K. Hong, J. Lee, W. Lee, S.-G. Kim, and C.-J. Choi, "Electronic structure and maximum energy product of MnBi," *Metals*, vol. 4, no. 3, pp. 455–464, Aug. 2014, doi: 10.3390/met4030455.

[25] W. Zhang, P. Kharel, S. Valloppilly, L. Yue, and D. J. Sellmyer, "High-energy-product MnBi films with controllable anisotropy," *Phys. Status Solidi (B)*, vol. 252, no. 9, pp. 1934–1939, Sep. 2015, doi: 10.1002/pssb.201552075.

[26] W. Tang, G. Ouyang, X. Liu, J. Wang, B. Cui, and J. Cui, "Engineering microstructure to improve coercivity of bulk MnBi magnet," *J. Magn. Magn. Mater.*, vol. 563, Dec. 2022, Art. no. 169912, doi: 10.1016/j.jmmm.2022.169912.

[27] C.-C. Huang, C.-C. Mo, G.-M. Chen, H.-H. Hsu, and G.-J. Shu, "Investigation on the La replacement and little additive modification of high-performance permanent magnetic strontium-ferrite," *Processes*, vol. 9, no. 6, p. 1034, Jun. 2021, doi: 10.3390/pr9061034.

[28] J. Cui et al., "Current progress and future challenges in rare-Earth-free permanent magnets," *Acta Mater.*, vol. 158, pp. 118–137, Oct. 2018, doi: 10.1016/j.actamat.2018.07.049.

[29] N. Kim et al., "Geometric effects in cylindrical core/shell hard–soft exchange-coupled magnetic nanostructures," *J. Magn. Magn. Mater.*, vol. 523, Apr. 2021, Art. no. 167599, doi: 10.1016/j.jmmm.2020.167599.

[30] X. Liu, S. Zuo, H. Wang, T. Zhang, Y. Dong, and C. Jiang, "Oriented exchange-coupled $L1_0$-FePt/Co core-shell nanoparticles with variable Co thickness," *RSC Adv.*, vol. 12, no. 12, pp. 7568–7573, Mar. 2022, doi: 10.1039/d1ra09304e.

[31] O. T. L. Traistaru, P. Shyam, M. Christensen, and S. P. Madsen, "Optimizing the energy product of exchange-coupled soft/hard $Zn_{0.2}Fe_{2.8}O_4$/$SrFe_{12}O_{19}$ magnets," *J. Appl. Phys.*, vol. 132, no. 16, Oct. 2022, Art. no. 163904, doi: 10.1063/5.0103242.